Graphene-based mid-infrared, tunable, electrically controlled plasmonic filter

2014 Appl. Phys. Express 7 024301

(http://iopscience.iop.org/1882-0786/7/2/024301)

Applied Physics Express 7, 024301 (2014)
http://dx.doi.org/10.7567/APEX.7.024301

Graphene-based mid-infrared, tunable, electrically controlled plasmonic filter

Hong-Ju Li[1], Ling-Ling Wang[1]*, Han Zhang[2], Zhen-Rong Huang[1], Bin Sun[1], Xiang Zhai[1], and Shuang-Chun Wen[2]

[1]School of Physics and Microelectronics and Key Laboratory for Micro–Nano Physics and Technology of Hunan Province, Hunan University, Changsha 410082, China
[2]Key Laboratory for Micro-/Nano-Optoelectronic Devices of Ministry of Education, College of Physics and Microelectronic Science, Hunan University, Changsha 410082, P. R. China
E-mail: llwang@hnu.edu.cn

Received November 29, 2013; accepted December 17, 2013; published online January 8, 2014

A planar plasmonic filter consisting of two graphene ribbons coupled by a graphene ring is constructed on monolayer graphene and investigated using the finite-difference time-domain method. The simulation results reveal that the edge modes indeed enhance the electromagnetic coupling between objects. The structure exhibits perfect band-pass filtering effect tuning and is optimized by means of the gate voltage. The simulation results are confirmed by the resonance theory of the ring. This structure is a real electrically controlled filter operating in the mid-infrared region. Our studies support the fabrication of ultracompact planar devices for optical processing. © 2014 The Japan Society of Applied Physics

Surface plasmon polaritons (SPPs),[1] the coupling between the collective excitation of free electrons in a metal and electromagnetic waves, propagate along the metal–dielectric interface. Because they can overcome the traditional diffraction limit and engineer light, surface plasmons in noble metals have been widely studied in past decades.[2–6] For example, optical amplifiers,[2] slow waveguides,[3] and reflectors,[4] have been reported in detail. However, the performance of metals is hampered because of the difficulty in varying and controlling their permittivity functions and the existence of material losses. Thus, the functionality of some metallic plasmonic devices is extremely constrained, especially in the infrared region. Because of these drawbacks, graphene,[7–10] a promising material for new-generation nanoplasmonic devices, has become notably popular because of its remarkable optical properties, including extreme confinement, advantageous tunability, and low losses.[11] In particular, its gate-voltage-dependent optical properties,[12,13] which were verified theoretically and experimentally, are emerging as a possible platform for electrically controlled plasmonic devices. Because the complex conductivity of graphene depends on the chemical potential, and the chemical potential can be controlled by the gate voltage, electric field, magnetic field, and chemical doping, we can create certain desired conductivity patterns on a single flake of graphene by using different values of the gate voltage at different locations. The corresponding waveguide devices have been achieved on monolayer graphene.[14,15] On the basis of the gate-voltage-dependent properties, optical splitters,[16] spatial switches,[17] and ultracompact Mach–Zehnder interferometers[18] have also been designed and exhibit better tunability than devices consisting of noble metals. In addition, the other recent research focus is the study of the SPP modes supported by graphene ribbons.[19,20] Remarkably, significant edge modes[21–23] in which the field is concentrated on the rims of graphene ribbons have been comprehensively reported; in particular, they may enhance the electromagnetic (EM) coupling between objects. Hence, they will play a significant role in planar integrated circuits.

Considering the two noteworthy facts mentioned above, we are impressed to find that it is feasible to create the desired planar plasmonic devices on a single flake of graphene. Hence, we propose an original planar filter consisting of two graphene nanoribbons coupled by a graphene ring.[24,25] It can be constructed on monolayer graphene by means of a split gate device that applies different bias voltages to different locations. We numerically investigate this structure using the finite-difference time-domain (FDTD) method.

The simulation results reveal that the edge modes can indeed enhance the EM coupling between objects, and the structure exhibits a perfect band-pass filtering effect. The size of the graphene ring is changed by varying the locations of the gate voltages on a single flake of graphene to tune the transmission spectrum. The FDTD results are verified by the resonance theory of the ring. By applying the same principle, the transmission spectrum is also optimized by changing the coupling length. Thus, using only the gate voltage, the transmission spectrum can be modified dynamically, and this method of realizing tunability is preferable to fabricating a new structure, which would be required for metallic devices. The proposed structure is a real electrically controlled plasmonic filter operating in the mid-infrared region. Our studies will play a substantial role in the fabrication of ultracompact, versatile planar devices in nano-integrated circuits for optical processing.

First, the characteristics of the SPP modes propagating along a graphene nanoribbon embedded in air were investigated numerically using the FDTD method with a perfectly matched layer absorbing boundary conditions. In inset (a) of Fig. 1, a graphene nanoribbon with a narrow width W and length L (in the x-direction) is modeled as an ultrathin film with a thickness of $\Delta = 1$ nm (in the z-direction). The surface conductivity (σ_g) of graphene is governed by the Kubo formula,[26] which depends on the momentum relaxation time τ, temperature T, chemical potential μ_c, and incident wavelength λ (frequency ω). At room temperature, the Kubo equation is reduced to[18]

$$\sigma_g = \frac{ie^2\mu_c}{\pi\hbar^2(\omega + i\tau^{-1})},$$

where the intraband transition dominates. The equivalent permittivity of graphene is calculated by the equation $\varepsilon_{eq} = 1 + i\sigma_g\eta_0/(k_0\Delta)$, where η_0 ($\approx 377\,\Omega$) is the intrinsic impedance of air, and $k_0 = 2\pi/\lambda$. A single graphene ribbon is well known to support two types of SPP modes: waveguide modes, in which the field is concentrated along the entire area of the ribbon (in the y-direction), and edge modes, in which the field is concentrated on the rims of the ribbon. Unlike the waveguide modes, which are used mainly for information

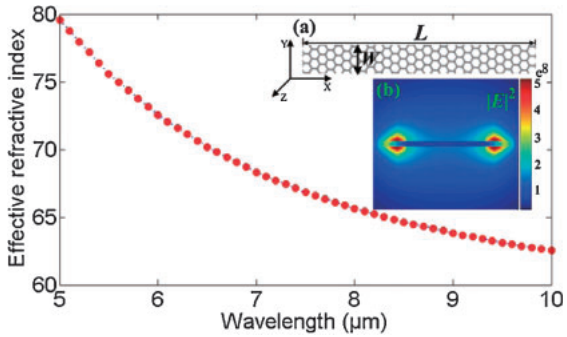

Fig. 1. Effective refractive indices of the SPP modes supported by a freestanding graphene ribbon as a function of incident wavelength λ. Inset (a) show graphene ribbon with $W = 20$ nm and $L = 300$ nm; inset (b) shows the field ($|E|^2$) distributions of the SPPs related to the y–z cross section of the graphene ribbons at $\lambda = 10$ μm.

transmission, the edge modes may be more conducive to EM coupling between objects.[22)]

However, the number of SPP modes supported by the nanoribbon increases as the ribbon width increases. When the width is ultrathin, for example, only dozens of nanometers, the ribbon supports only the fundamental edge modes in the mid-infrared region. As shown in inset (a) of Fig. 1, where the microscopic details at the edges of the graphene ribbon are ignored, the width W and length L are assumed to be 20 and 300 nm, respectively. The other material parameters of τ and μ_c, which directly affect the surface conductivity of graphene, are set to 0.5 ps and 0.3 eV, respectively. SPP waves are excited by a dipole point source placed 2 nm above the ribbon in the z-direction and have the form $\boldsymbol{E}_{(r,\omega,t)} = \boldsymbol{E}_{(y,z)} \exp(ik_x(\omega)x - i\omega t)$ where $k_x(\omega)$ is the wave vector in the propagation direction x. The corresponding effective refractive indices calculated by $n_{\text{eff}} = \text{Re}[k_x(\omega)]/k_0$ are also illustrated in Fig. 1. At the same time, the contour profiles of $|E|^2$ in the y–z cross section clearly reveal that most of the field energy is indeed concentrated on the rims of the graphene ribbon, as shown in inset (b), where the incident wavelength λ is 10 μm. Therefore, the ultranarrow graphene ribbon with $W = 20$ nm supports only the fundamental edge modes. The results are in accordance with the above theoretical analysis.

Because the ultranarrow graphene ribbon supports only the edge mode, which may facilitate EM coupling between objects, we made full use of this feature to fabricate a filter structure of two graphene nanoribbons coupled by a graphene ring resonator. It can also be designed on monolayer graphene by means of a split gate device that applies different bias voltages to different locations to create non-uniform conductivity patterns. As displayed in Fig. 2, only the red zones with the gate voltage value V_2 are capable of supporting SPPs, and the other zones, with V_1, behave as dielectrics and do not support SPPs. In Fig. 2, the length of the graphene waveguide is L and the width is W, which is the same as the width of the graphene ring. The outer radius of the ring resonator is R, and the coupling length between the waveguides and the ring resonator is d. Certainly, in addition to using a split gate device to apply different bias voltages to different locations, other ways of realizing inhomogeneous conductivity patterns across a single graphene layer have also been used, including an uneven ground plane holding the

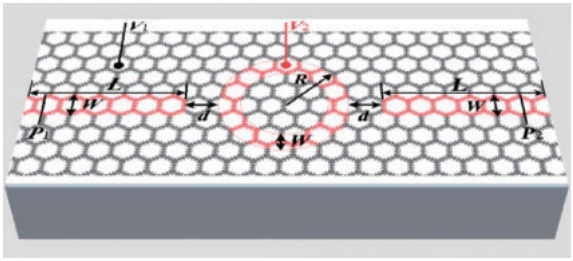

Fig. 2. Schematic diagram of the planar band-pass filter structure consisting of two graphene waveguides coupled by a graphene ring resonator, which is constructed on monolayer graphene in which only the red areas with the gate voltage value V_2 support SPPs, and the others do not.

monolayer graphene and a non-uniform permittivity distribution underneath the graphene sheet.[14)]

The proposed structure is investigated using the FDTD method. For simplicity, our calculations consider graphene ribbons coupled by a graphene ring embedded in air. In the implementation, we use a non-uniform mesh. The minimum mesh size inside the graphene layer equals 0.1 nm and gradually increases outside the graphene sheet to reduce the storage space and computational time. Similarly, one dipole point source placed 2 nm above the left ribbon is used to excite the SPP waves. Monitors are placed at points P_1 and P_2 to detect the incident power P_{in} and transmitted power P_{out}. The transmission is defined as $T = P_{\text{out}}/P_{\text{in}}$. The material parameters are unchanged, and the structural parameters of L, W, d, and R, are assumed to be 300, 20, 5, and 45 nm, respectively. The simulation results corresponding to different incident wavelengths are presented in Fig. 3.

Considering this structure, it is well known that the SPPs excited in the left graphene waveguide will travel clockwise and anticlockwise simultaneously in the ring and be transmitted from the right waveguide. Only those incident wavelengths satisfying the resonance condition of the ring can be transported efficiently, whereas others are stopped. Therefore, in Fig. 3(a), two pronounced transmission peaks corresponding to wavelengths of $\lambda = 7.8$ μm and 6.2 μm appear in the transmission spectrum, exhibiting an obvious band-pass filtering effect in the mid-infrared region. Moreover, Figs. 3(b) and 3(c) display the contour profiles of the field H_z of the filter structure at incident wavelengths of $\lambda = 7.8$ and 6.2 μm, respectively, which are related to the transmission peaks shown in Fig. 3(a). Clearly, a second-order resonance is formed in the graphene ring resonator at $\lambda = 7.8$ μm, and a third-order resonance is formed at $\lambda = 6.2$ μm. The edge modes propagate along the graphene ribbon perfectly and indeed enhance the EM coupling between the waveguides and the ring.

Next, we investigated the influence of the graphene ring's outer radius on the wavelengths of the transmission peaks. On the same principle as that shown in Fig. 2, we can vary the locations with the gate voltage value V_2 to change the size of the ring, which is unlike the conventional method of fabricating a new structure. The simulation results are presented in Fig. 4(a). The transmission spectra plotted in black, blue, red, and green lines correspond to graphene rings with outer radii of 45, 50, 55, and 60 nm, respectively. A comparison of the curves in Fig. 4(a) shows that the transmission peaks with the same order tend to exhibit a redshift as the outer radius

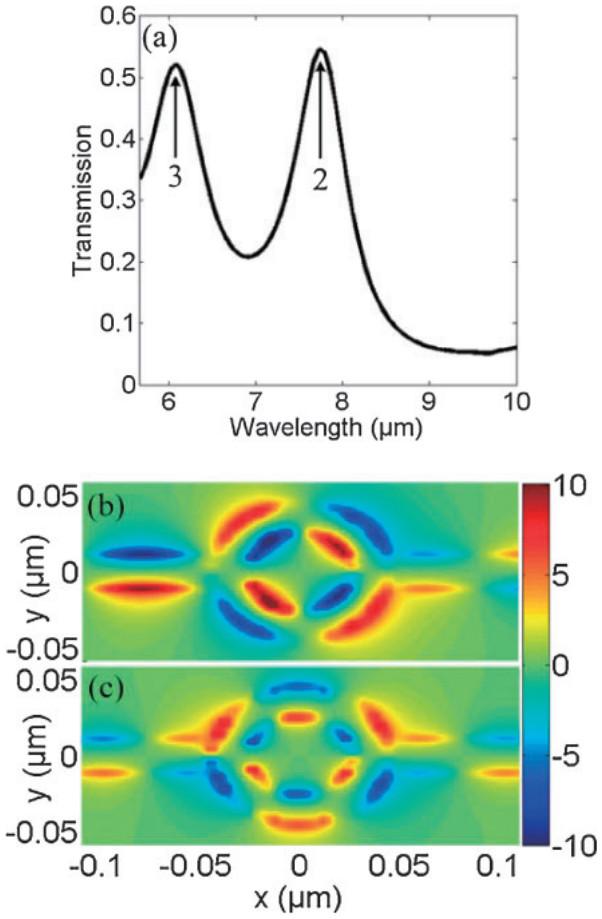

Fig. 3. (a) Transmission spectrum of proposed structure. Contour profiles of field H_z of the filter structure at different incident wavelengths of (b) $\lambda = 7.8\,\mu m$ and (c) $\lambda = 6.2\,\mu m$.

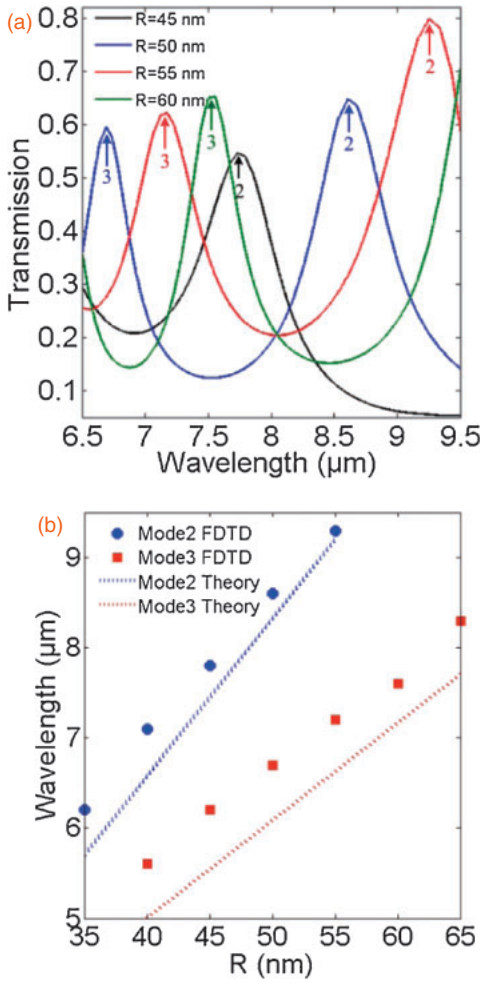

Fig. 4. (a) Transmission spectra for different outer radii of the graphene rings. (b) Wavelengths of the transmission peaks as a function of the outer radius of the graphene ring.

increases, and the entire transmission spectrum exhibits obvious tunability. The relationship between the wavelengths of the transmission peaks and the outer radii is related to the resonance equation of the ring,[27]

$$\frac{J_n'(kR)}{J_n'(kr)} - \frac{N_n'(kR)}{N_n'(kr)} = 0,$$

where $k = k_0 \cdot n_{\text{eff}}$, and n_{eff} is the effective refraction index (ERI) of the graphene ring; $r = R - W$ is the inner radius of the ring resonator. J_n' is the derivative of the Bessel function of the first kind with order n, and N_n' is the derivation of the Bessel function of the second kind with order n. The second- and third-order resonance modes, i.e., modes 2 and 3, correspond to the second- and third-order Bessel and Hankel functions, respectively. According to this equation, as the outer radius increases, the resonance wavelengths indeed tend to exhibit a redshift. The theoretical results are in agreement with the FDTD results shown in Fig. 4(b). In Fig. 4(b), only a slight difference appears between the theoretical and FDTD results because the ERI is assumed to be the same in the entire ring. In fact, the ERI in the coupled areas differs from that in the other areas of the ring because the coupling length is finite. Thus, the transmission spectrum can be tuned dynamically on a single flake of graphene by varying the locations with the gate voltage V_2 to change the size of the ring. An electrically controlled plasmonic device is achieved, and this simpler method is preferable for realizing tunability instead of directly fabricating a new structure, as would be needed for metallic devices.

Finally, we modified the transmission spectrum by tuning the coupling length d. In Fig. 2, the locations with the gate voltage V_2 on the ring are unchanged, and the locations on the two graphene waveguides are varied to tune d. The simulation results are presented in Fig. 5, where R is constant at 45 nm. In Fig. 5(a), the coupling length clearly has little effect on the wavelengths of the transmission peaks because the resonance wavelengths are unrelated to the coupling length according to the above resonance equation. As the coupling length increases, the full width at half-maximum (FWHM) of the transmission spectra decreases, as shown in Fig. 5(b), which shows the dependence of the FWHM of mode 2 on the coupling length. At the same time, because the coupling losses increase with increasing coupling length, the maximum transmission decreases gradually, and the height difference (HD) of the transmission peak is changed correspondingly, as shown in Fig. 5(b). Thus, the coupling length affects the quality of the transmission peaks. However, it is better to obtain transmission peaks with a smaller FWHM and larger HD. Among the five curves in Fig. 5(a), the transmission spectrum with $d = 9\,nm$ is optimal. Certainly, we can also optimize the transmission spectrum to meet different needs by engineering the locations of the

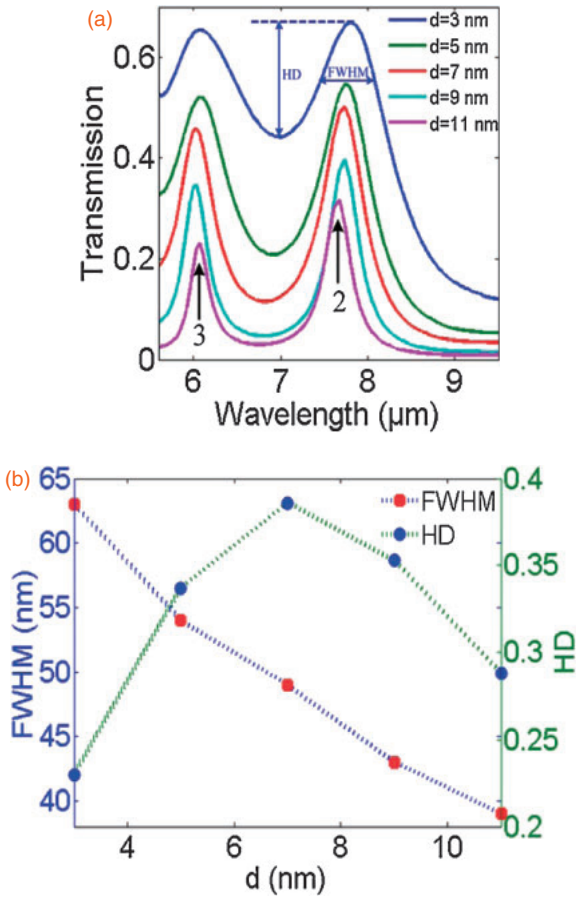

Fig. 5. (a) Transmission spectra for different coupling lengths with same outer radius. (b) Dependence of FWHM and HD of mode 2 on coupling length *d*.

gate voltage to change the coupling length. This will be more convenient in practical applications.

In conclusion, a planar plasmonic filter consisting of two graphene ribbons coupled by a graphene ring was proposed and investigated numerically using the FDTD method. It can also be constructed on monolayer graphene using a split gate device to apply different bias voltages to different locations. Simulation results reveal that the edge modes supported by the graphene nanoribbons indeed enhanced the EM coupling between objects, and the structure exhibited a perfect band-pass filtering effect. The size of the ring is changed by varying the locations of the gate voltages to tune the transmission spectrum. The FDTD results are verified by the resonance theory of the ring. According to the same principle, the transmission spectrum is also optimized by changing the coupling length. This gate voltage method of tunability is preferable to that used in conventional metallic devices, and the proposed structure is a real electrically controlled plasmonic filter operating in the mid-infrared region. Our studies will play a significant role in the fabrication of ultracompact planar devices for optical processing.

Acknowledgments This work was supported by the National Natural Science Foundation of China (Grant Nos. 11074069, 61176116, and 11264021), the Specialized Research Fund for the Doctoral Program of Higher Education of China (Grant No. 20120161130003), and the Aid program for Science and Technology Innovative Research Team in Higher Educational Institutions of Hunan Province.

1) W. L. Barnes, A. Dereux, and T. W. Ebbesen, Nature **424**, 824 (2003).
2) I. De Leon and P. Berini, Nat. Photonics **4**, 382 (2010).
3) G. Wang, H. Lu, and X. Liu, Appl. Phys. Lett. **101**, 013111 (2012).
4) Y. Gong, L. Wang, X. Hu, X. Li, and X. Liu, Opt. Express **17**, 13727 (2009).
5) G. Gómez-Santos and T. Stauber, EPL **99**, 27006 (2012).
6) Y. Wang, J. Wang, S. Gao, and C. Liu, Appl. Phys. Express **6**, 022003 (2013).
7) F. Bonaccorso, Z. Sun, T. Hasan, and A. C. Ferrari, Nat. Photonics **4**, 611 (2010).
8) A. K. Geim and K. S. Novoselov, Nat. Mater. **6**, 183 (2007).
9) H. Kageshima, H. Hibino, M. Nagase, and H. Yamaguchi, Appl. Phys. Express **2**, 065502 (2009).
10) H. Zhang, Q. Bao, D. Tang, L. Zhao, and K. Loh, Appl. Phys. Lett. **95**, 141103 (2009).
11) Q. Bao and K. P. Loh, ACS Nano **6**, 3677 (2012).
12) J. Chen, M. Badioli, P. Alonso-González, S. Thongrattanasiri, F. Huth, J. Osmond, M. Spasenović, A. Centeno, A. Pesquera, P. Godignon, A. Z. Elorza, N. Camara, F. J. García de Abajo, R. Hillenbrand, and F. H. L. Koppens, Nature **487**, 77 (2012).
13) Z. Fei, A. S. Rodin, G. O. Andreev, W. Bao, A. S. McLeod, M. Wagner, L. M. Zhang, Z. Zhao, M. Thiemens, G. Dominguez, M. M. Fogler, A. H. Castro Neto, C. N. Lau, F. Keilmann, and D. N. Basov, Nature **487**, 82 (2012).
14) A. Vakil and N. Engheta, Science **332**, 1291 (2011).
15) Yu. V. Bludov, M. I. Vasilevskiy, and N. M. R. Peres, EPL **92**, 68001 (2010).
16) H. Lin, M. F. Pantoja, L. D. Angulo, J. Alvarez, R. G. Martin, and S. G. Garcia, IEEE Microwave Wireless Components Lett. **22**, 612 (2012).
17) H. Li, L. Wang, Z. Huang, B. Sun, X. Zhai, and X. Li, EPL **104**, 37001 (2013).
18) B. Wang, X. Zhang, X. Yuan, and J. Teng, Appl. Phys. Lett. **100**, 131111 (2012).
19) W. Gao, J. Shu, C. Qiu, and Q. Xu, ACS Nano **6**, 7806 (2012).
20) D. Utsugi, C. Hu, and K. Watanabe, Appl. Phys. Express **5**, 105101 (2012).
21) J. Christensen, A. Manjavacas, S. Thongrattanasiri, F. H. L. Koppens, and F. J. García de Abajo, ACS Nano **6**, 431 (2012).
22) A. Y. Nikitin, F. Guinea, F. J. García-Vidal, and L. Martín-Moreno, Phys. Rev. B **84**, 161407 (2011).
23) X. Zhu, W. Yan, N. A. Mortensen, and S. Xiao, Opt. Express **21**, 3486 (2013).
24) N. Papasimakis, S. Thongrattanasiri, N. I. Zheludev, and F. J. García de Abajo, Light Sci. Appl. **2**, e78 (2013).
25) P. Liu, W. Cai, L. Wang, X. Zhang, and J. Xu, Appl. Phys. Lett. **100**, 153111 (2012).
26) P.-Y. Chen and A. Alù, ACS Nano **5**, 5855 (2011).
27) T.-B. Wang, X.-W. Wen, C.-P. Yin, and H.-Z. Wang, Opt. Express **17**, 24096 (2009).